DOE/ET/53088--370

DE89 016618

Stability of the Global Alfvén Eigenmode in the Presence of Fusion Alpha Particles in an Ignited Tokamak Plasma

G.Y. Fu* and J.W. Van Dam
Institute for Fusion Studies and *Center for Fusion Engineering
The University of Texas at Austin
Austin, TX 78712

Abstract

The stability of the Global Alfvén Eigenmodes is investigated in the presence of super-Alfvénic energetic particles, such as the fusion-product alpha particles in an ignited deuterium-tritium tokamak plasma. Alpha particles tend to destabilize these modes when $\omega_{*\alpha} > \omega_A$, where ω_A is the shear-Alfvén modal frequency and $\omega_{*\alpha}$ is the alpha particle diamagnetic drift frequency. This destabilization due to alpha particles is found to be significantly enhanced when the alpha particles are modeled with a slowing-down distribution function rather than with a Maxwellian. However, previously neglected electron damping due to the magnetic curvature drift is found to be comparable in magnitude to the destabilizing alpha particle term. Furthermore, the effects of toroidicity are also found to be stabilizing, since the intrinsic toroidicity induces poloidal mode coupling, which enhances the parallel electron damping from the sideband shear-Alfvén Landau resonance. In particular, for the parameters of the proposed Compact Ignition Tokamak, the Global Alfvén Eigenmodes are found to be completely stabilized by either the electron damping that enters through the magnetic curvature drift or the damping introduced by finite toroidicity.

---

1 Introduction

Recently the effects of energetic particles on magnetohydrodynamic (MHD) modes have been studied extensively. In the neutral beam heating experiments on the Princeton Divertor Experiment,[1] the injected energetic trapped particles are thought to have been responsible for destabilizing the internal kink mode and causing fishbone instabilities.[2] Subsequently, ballooning modes were also found to be destabilized by the same group of hot particles, thus serving as an explanation for the high-frequency fishbone precursor oscillations that were experimentally observed.[3,4] Furthermore, it has been shown that both the ballooning mode[5] and the internal kink mode[6–8] can be stabilized by hot particles of even higher energy. However, at these high energies, some new instabilities may occur: in particular, the shear-Alfvén waves may be destabilized by super-Alfvénic energetic particles through the inverse Landau damping process if $\omega_* > \omega_A$, where ω_A is the shear-Alfvén frequency and ω_* is the diamagnetic drift frequency of the energetic particle species. This condition can readily be satisfied by fusion alpha particles in an ignited deuterium-tritium tokamak plasma since these alpha particles are born with an energy of 3.52 Mev and have a density profile that is sharply peaked at the center of the plasma due to the sensitive dependence of the fusion reaction cross section on the plasma temperature.

In the ideal MHD description with cylindrical geometry, the shear-Alfvén wave in a nonuniform plasma satisfies a second-order differential equation that admits a continuous spectrum[9,10] for ω^2 over the range of $(\omega_A^2)_{\min} < \omega^2 < (\omega_A^2)_{\max}$, where $\omega_A = k_{||} v_A$ is a function of the minor radius, $k_{||}$ is the parallel wave number, and $v_A = B/(4\pi n_i m_i)^{1/2}$ is the Alfvén velocity, with $n_i m_i$ the ion mass density. With the inclusion of parallel electron response and finite ion Larmor radius, the continua become closely spaced, discrete spectra. The corresponding eigenmodes, which are localized around the Alfvén resonances, are called

Kinetic Alfvén Waves (KAW).[11] Recently, extensive theoretical and experimental studies[12–17] have revealed the existence of discrete eigenmodes just below the lower edge of the Alfvén continuum, i.e., $\omega^2 < (\omega_A^2)_{\min}$. These modes are regular global MHD modes extending over the plasma minor radius and are called Global Alfvén Eigenmodes (GAE).

The destabilization of shear-Alfvén waves was first studied by Mikhailovskii,[18] using a local dispersion relation. By including finite Larmor radius effects to discretize the continuum, Rosenbluth and Rutherford[19] found that the KAW can be destabilized by alpha particles. Tsang *et al.*[20] studied the details of the same problem numerically and reached a similar conclusion. More recently, Li *et al.*[21] found that GAE can also be destabilized by fusion alpha particles in a burning tokamak plasma.

In the present work, we study the stability of GAE modes in the presence of fusion alpha particles in an ignited tokamak plasma. We first examine the GAE modes in the cylindrical geometry approximation. We show that the alpha particle-induced growth rate is enhanced significantly when the alpha particles are modeled in terms of a slowing-down distribution function, rather than with a Maxwellian distribution. A preliminary version of this result, derived analytically, was noted earlier,[4] along with numerical confirmation.[4,21] However, previous work[4,21] neglected the electron and ion contribution to the perturbed current due to the magnetic curvature drift; only the alpha particle contribution, which destabilizes the GAE modes through inverse Landau damping, was kept. In the present work we also find that the electron curvature drift term is always stabilizing since the electron diamagnetic drift frequency is much smaller than the Alfvén frequency. More importantly, this electron term is comparable in magnitude to the alpha particle term. The reason is that the electron density is much higher than that of the alpha particles, even though the electron velocity is much larger than the Alfvén phase velocity and the alpha particle energy is much higher than the electron temperature.

Second, we consider the effects of toroidicity on the stability of the GAE modes. Previous

work[21] only considered a single poloidal mode and neglected the intrinsic poloidal mode coupling that is induced by toroidicity. Shown in Fig. 1 are the shear Alfvén continua in cylindrical geometry for toroidal mode number $n = 1$ and poloidal mode numbers $m = -1, -2$, and -3. In particular, the eigenfrequency of the cylindrical GAE with mode $(n, m) = (1, -2)$ is located just below the minimum of the $m = -2$ continuum, as indicated by the dotted line. In toroidal tokamak geometry, the cylindrical $(1, -2)$ mode will be coupled to sidebands, especially the $(1, -3)$ poloidal mode and the $(1, -1)$ mode, as well as other more distant poloidal modes. In particular, we observe that the sideband $(1, -1)$ mode has an Alfvén resonance near the edge of the plasma. We will find that this Alfvén resonance enhances the parallel electron Landau damping and has a stabilizing effect. In particular, for parameters corresponding to those proposed for the Compact Ignition Tokamak (CIT), we find that the GAE modes are completely stabilized.

The outline of this paper is as follows. In Sec. 2 of this paper, we consider the stability of the GAE modes in the cylindrical limit. We study the effects of using a slowing-down distribution function, rather than a Maxwellian, to model the fusion-product alpha particles. We also discuss the effect of the electron magnetic curvature drift on the stability of the GAE modes. Section 3 examines the stability of the GAE modes in a toroidal device. First we construct a toroidal eigenmode equation for the GAE modes, and then the numerical results are presented. Finally, Sec. 4 is devoted to conclusions and discussion.

2 Stability of the GAE in the Cylindrical Limit

2.1 Review of GAE Destabilization by Alpha Particles

Here we give a unified overview of the cylindrical results for the destabilization of the GAE mode by alpha particles. The proper set of eigenmode equations for the cylindrical problem

has been previously derived by Li, Mahajan, and Ross,[21] who started from Ampére's law:

$$\nabla \times \nabla \times \mathbf{E} = \left(\frac{\omega^2}{c^2}\right) \boldsymbol{\chi} \cdot \mathbf{E} \,. \tag{1}$$

All the physics of the plasma response is included in the susceptibility tensor $\boldsymbol{\chi}$. An ignited tokamak plasma has two components: the bulk plasma, which constitutes one component, has relatively high density and low temperature, whereas the fusion-product alpha particles, which are the other component, have low density and high temperature. Accordingly, the susceptibility has two parts, i.e., $\boldsymbol{\chi} = \boldsymbol{\chi}_c + \boldsymbol{\chi}_\alpha$, where $\boldsymbol{\chi}_c$ and $\boldsymbol{\chi}_\alpha$ come from the bulk plasma component and the hot alpha particle component, respectively. From the well-known low-frequency ($\omega < \omega_{ci}$) susceptibility tensor for a uniform plasma, a simple self-adjoint $\boldsymbol{\chi}_c$ for the nonuniform cold plasma may be constructed,[13] including all the important kinetic effects. The form for $\boldsymbol{\chi}_\alpha$, on the other hand, is obtained[21] from the solution of the drift kinetic equation for circulating alpha particles (the effect of trapped particles being neglected). Furthermore, it is convenient to decompose the electric field $\mathbf{E}$ into $\mathbf{E} = E_r \mathbf{r} + E_\perp \mathbf{b} \times \mathbf{r} + E_\parallel \mathbf{b}$ where $\mathbf{b} = \mathbf{B}/B$ is the unit vector along the magnetic field $\mathbf{B}$ and $\mathbf{r}$ is the unit vector in the radial direction. Also, the parallel component of Ampére's law is replaced by $\nabla \cdot \mathbf{J} = 0$, which in turn enables us to eliminate $E_\parallel$ in terms of E_r and $E_\perp$. Thus, from the other two components of Ampére's law, we have the following two second-order differential equations, written in matrix form as

$$\tilde{L}\tilde{E} \equiv \begin{pmatrix} L_{rr} & L_{r\perp} \\ L_{\perp r} & L_{\perp\perp} \end{pmatrix} \begin{pmatrix} E_r \\ E_\perp \end{pmatrix} = 0 \tag{2}$$

where $\tilde{L}$ is a differential matrix operator with the following elements:

$$\begin{aligned} L_{rr} \;=\; & \frac{\omega^2}{v_A^2} - k_\parallel^2 - k_\perp^2 - \frac{11}{8} b_i \, k_\perp^2 + \frac{d}{dr} \frac{3}{8} b_i \frac{1}{r} \frac{d}{dr} r \\ & + k_\parallel \frac{d}{dr} \, k_\parallel^{-1} d_e \frac{v_A^2}{\omega^2} \frac{1}{r} \frac{d}{dr} r \frac{\omega^2}{v_A^2} + S_{rr} - Q_{m-1} - Q_{m+1} \end{aligned} \tag{3}$$

$$L_{r\perp} = i\left[-\frac{k_\perp}{r}\frac{d}{dr}r - \frac{k_\perp}{r}\frac{11}{8}b_i\frac{d}{dr}r + \frac{d}{dr}\frac{3}{8}b_i\,k_\perp \right.$$
$$\left. + k_\parallel \frac{d}{dr}\,k_\parallel^{-1} d_e\,k_\perp - iS_{r\perp} + Q_{m-1} - Q_{m+1}\right] \tag{4}$$

$$L_{\perp\perp} = \frac{\omega^2}{v_A^2} - k_\parallel^2 + \frac{d}{dr}\frac{1}{r}\frac{d}{dr}r + \frac{d}{dr}\frac{11}{8}b_i\frac{1}{r}\frac{d}{dr}r - \frac{3}{8}b_i\,k_\perp^2$$
$$- d_e\,k_\perp^2 + S_{\perp\perp} - Q_{m-1} - Q_{m+1} \tag{5}$$

$$L_{\perp r} = -i\left[-\frac{d}{dr}k_\perp - \frac{d}{dr}\frac{11}{8}b_i\,k_\perp + k_\perp\frac{3}{8}b_i\frac{1}{r}\frac{d}{dr}r \right.$$
$$\left. + k_\perp d_e\frac{v_A^2}{\omega^2}\frac{1}{r}\frac{d}{dr}r\frac{\omega^2}{v_A^2} - iS_{\perp r} - Q_{m-1} + Q_{m+1}\right]\ . \tag{6}$$

Here $b_i = (\omega^2/v_A^2)\rho_i^2$ and $d_e = (k_\parallel\rho_s)^2\left[1 + (\omega/k_\parallel v_e)Z(\omega/k_\parallel v_e)\right]^{-1}$, with $\rho_i^2 = 2T_i/m_i\omega_{ci}^2$ the ion Larmor radius, $\rho_s^2 = T_e/m_i\omega_{ci}^2$, ω_{ci} the ion cyclotron frequency, ω the frequency of the perturbed field, and v_e the electron thermal velocity. The wave numbers are given approximately by $k_\perp = m/r$ and $k_\parallel = (n - m/q)/R$, where n and m are the toroidal mode number and the poloidal mode number, respectively, and R is the major radius. The terms S_{rr}, $S_{r\perp}$, $S_{\perp\perp}$, and $S_{\perp r}$, which arise from the equilibrium current and the shear of the magnetic field, are given in Ref. 13, and the term $Q_{m\pm1}$ is the alpha particle contribution given in Eqs. (24) and (25) of Ref. 21 as follows:

$$Q_{m\pm1} = -i\frac{\beta_\alpha}{2R^2}\left(P_{m\pm1} - \frac{\omega_{*\alpha m}}{\omega}R_{m\pm1}\right) \tag{7}$$

$$P_{m\pm1} = \frac{\pi\omega}{v_\alpha^4}\int d^3v\left(v_\perp^2/2 + v_\parallel^2\right)^2\left(-T_\alpha\frac{\partial f_{\alpha0}}{\partial\epsilon}\right)\delta(\omega - k_\parallel v_\parallel) \tag{8}$$

$$R_{m\pm1} = \frac{\pi\omega}{v_\alpha^4}\int d^3v\left(v_\perp^2/2 + v_\parallel^2\right)^2 f_{\alpha0}\delta(\omega - k_\parallel v_\parallel)\ . \tag{9}$$

Here, $\beta_\alpha = 8\pi n_\alpha T_\alpha / B^2$ and $v_\alpha^2 = 2T_\alpha/m_\alpha$, with T_α, n_α, β_α, and v_α being the temperature, density, beta value, and thermal velocity of the alpha particles, respectively. Also, $f_{\alpha 0}$ is the alpha particle equilibrium distribution function. Notice that in the alpha particle terms, the wave-particle Landau-type parallel resonance is of the form $\omega = k_{\|m\pm1} v_{\|\alpha}$, rather than $\omega = k_{\|m} v_{\|\alpha}$; i.e., the alpha particles resonantly interact with the sideband of the perturbed field. This occurs because the poloidal variation of the alpha particle magnetic drift velocity $\mathbf{v}_{d\alpha}$ enables the perpendicular fields $E_\perp$ and E_r of mode m to resonantly drive two sidebands, $m \pm 1$, of the perturbed alpha particle distribution. This kind of sideband resonance was vividly described by Mikhailovskii[18] — "A particle moving in a magnetic field with an alternating curvature and in the field of perturbation with longitudinal wave number $k_\|$ behaves as if it moved in a straight magnetic field and in a field of wave with an effective longitudinal wavenumber $k_{\|\text{eff}} = k_\| \pm 1/qR$." However, in the end, these two sidebands of the distribution contribute to a perturbed alpha particle magnetic drift current with the same poloidal mode number as that of the perturbed field. We conclude that toroidal coupling in the alpha particle response is necessary, even only one poloidal mode number is considered. This is the first manifestation of the effect of toroidicity in what is here taken to be an otherwise cylindrical problem. In Sec. 3, we will study the essential toroidal coupling due to the intrinsically finite value of the inverse aspect ratio (r/R), which drives various poloidal harmonics of the waves under consideration.

The physics of Eq. (2) can be briefly stated as follows. The b_i terms represent the effect of finite ion Larmor radius, whereas the d_e terms come from the electron parallel dynamics, which result in Landau damping. Without these b_i and d_e terms and the $Q_{m\pm1}$ terms, the matrix equation Eq. (2) can be combined into a single second-order differential equation, the coefficient of whose second derivative term vanishes at $\omega^2 = k_\|^2 v_A^2$: this admits a continuous spectrum. On the other hand, with these terms, a fourth-order equation results, and the spectrum is discretized. Furthermore, the alpha particle terms, $Q_{m\pm1}$, can lead to

an eigenfrequency with a positive imaginary part; i.e., the alpha particles are destabilizing. To understand this, it is useful to examine the simplest local dispersion relation, given by Eqs. (39) and (40) of Ref. 21. If one considers the case of a uniform background plasma density and a Maxwellian distribution for the alpha particles, the shear-Alfvén wave is described by

$$\frac{\omega^2}{v_A^2} - k_\parallel^2 - A_\alpha - (k_\perp^2 + k_r^2)d_e = 0 \tag{10}$$

where

$$\begin{aligned} A_\alpha &= (Q_{m+1} + Q_{m-1}) \\ &= -i\frac{\beta_\alpha}{2R^2}\left(1 - \frac{\omega_{*\alpha}}{\omega}\right)(R_{m+1} + R_{m-1}) \end{aligned} \tag{11}$$

The growth rate is then given analytically by the following expression:

$$\begin{aligned} \gamma/\omega_A &= -\frac{\beta_\alpha}{4k_\parallel^2 R^2}\left(1 - \frac{\omega_{*\alpha}}{\omega}\right)(R_{m+1} + R_{m-1}) \\ &\quad - \left(k_r^2 + k_\perp^2\right)\rho_s^2 \pi^{1/2}\frac{v_A}{v_e} \, . \end{aligned} \tag{12}$$

We observe that for $\omega_{*\alpha} > \omega$, the alpha term is destabilizing; this competes with the second term on the right-hand side of Eq. (12), i.e., the Landau damping. Also note that the Landau damping is proportional to $(k_r^2 + k_\perp^2)\rho_s^2$, so that for a global mode like GAE mode, the damping is very weak, whereas for the radially localized KAW modes with their large k_r, Landau damping can be quite large.

2.2 Slowing-Down Distribution Versus Maxwellian Distribution

Here we study the effect of using a slowing-down distribution on the destabilization of the GAE mode by alpha particles for typical ignition parameters, as compared to using a Maxwellian distribution for the alpha particles. The eigenmode equation, Eq. (2), can be

Table1: CIT tokamak parameters

major radius	R(cm)	140
minor radius	a(cm)	67
wall radius	r_w(cm)	85
toroidal field	B_0(T)	10
central electron density	$n_0(10^{14}/\text{cm}^3)$	10
central alpha particle density	$n_\alpha(0)(10^{13}/\text{cm}^3)$	2
central electron temperature	T_{e0}(kev)	30
central ion temperature	T_{i0}(kev)	30
effective mass	m_{eff}(proton mass)	2.5
effective charge	Z_{eff}(electron charge)	3.0

solved by the cubic-B spline finite element method. Shown in Fig. 2 are the GAE eigenfunctions for modes $(1,-2)$ and $(0,-2)$. Figure 3 gives the corresponding growth rates for both Maxwellian and slowing-down distributions. The parameters for one version of the proposed Compact Ignition Tokamak (CIT) have been used in the calculation; these are given in Table 1. The CIT profiles were taken to be the following:

$$n = n_0 \left[1 - r^2/(a+d)^2\right] \tag{13}$$

$$T_{e,i} = T_{0e,i} \left[1 - (r/a)^2\right] \tag{14}$$

$$q = 1 + 2(r/a)^2 \tag{15}$$

where the value of d is chosen such that the plasma density at the edge is 10% of its central value: $n(a)/n(0) = 0.1$. The alpha particle density profile is taken to be $n_\alpha(r) = n_\alpha(0)\exp(-r^2/L_\alpha^2)$, where L_α is the alpha particle density gradient scale length. Notice that the $(1,-2)$ mode is weakly damped for a Maxwellian distribution, but is slightly unstable for

a slowing-down distribution. However, for the $(0,-2)$ mode, which has been identified as the most unstable mode for TFTR parameters,[21] the effect of modeling the alpha particles with a slowing-down distribution is quite remarkable. We observe that the growth rate for a slowing-down distribution is about twice that for a Maxwellian distribution. More significantly, at the expected CIT alpha particle density scale length of $L_\alpha = 0.4a$, the mode is substantially unstable for a slowing-down distribution, but is stable for a Maxwellian distribution.

We can explain the difference in the results for the two distributions with the following estimate. For a Maxwellian distribution, we have $\partial f_\alpha/\partial E = -f_\alpha/T_\alpha$ so that $P_{m\pm1} = R_{m\pm1}$; on the other hand, for a slowing-down distribution we have $R_{m\pm1} > P_{m\pm1}$, since the velocity integral is heavily weighted toward high energy where $-T_\alpha \partial f_\alpha/\partial E \approx (3/2)(T_\alpha/E) f_\alpha > f_\alpha$ (Note that for CIT parameters we have $T_\alpha \approx 1$ Mev, where the maximum energy of the alpha particles is 3.52 Mev). Indeed, this has been borne out by our analytical results. Shown in Fig. 4 is the ratio of $R_{m\pm1}$ for the two distributions plotted versus the phase quantity $\omega/k_{\|m\pm1}v_{\alpha 0}$, along with the ratio of $P_{m\pm1}$ to $R_{m\pm1}$ for a slowing-down distribution. We observe that

$$(R_{m\pm1})_{\text{slowing-down}} \approx (R_{m\pm1})_{\text{Maxwellian}} \tag{16}$$

for $\omega/k_{\|m\pm1}v_{\alpha 0} < 0.8$ and, more interestingly, that

$$(P_{m\pm1})_{\text{slowing-down}} \approx \frac{1}{2}(R_{m\pm1})_{\text{slowing-down}} \ . \tag{17}$$

Hence, not surprisingly, the growth rate for a slowing-down distribution is greater than that for a Maxwellian, as has been shown in Fig. 3. It is also worthwhile to point out that we can estimate the ratio of the critical alpha scale length $L_{\alpha,\text{crit}}$ that corresponds to zero growth rate for the two distributions:

$$\frac{(L_{\alpha,\text{crit}})_{\text{slowing-down}}}{(L_{\alpha,\text{crit}})_{\text{Maxwellian}}} \approx \left(\sqrt{\frac{R_{m\pm1}}{P_{m\pm1}}}\right)_{\text{slowing-down}} \approx 1.4 \tag{18}$$

which is remarkably close when compared to the numerical results shown in Fig. 3(b), which

give

$$\frac{(L_{\alpha,\mathrm{crit}})_{\mathrm{slowing-down}}}{(L_{\alpha,\mathrm{crit}})_{\mathrm{Maxwellian}}} = \frac{0.47}{0.33} = 1.4 \ . \tag{19}$$

2.3 Electron Damping due to Curvature Drift

Previous work[4,19–21] only considered the contribution of the fusion alpha particles to the perturbed current that is due to the alpha particle magnetic curvature drift, which is destabilizing through the inverse Landau damping process. Similar terms for the electrons and ions were ignored since their drift velocities are much smaller than that of the alpha particles and their thermal velocities are very different from the Alfvén phase velocity. Nonetheless, here we will show that for GAE modes the electron contribution to the drift current term can indeed be comparable in magnitude to the alpha particle contribution. The reason is simply that the electron density is much higher than that of the alpha particles, especially away from the plasma center, although the electron temperature is much lower than the alpha particle temperature and the electron thermal velocity is much larger than the Alfvén phase velocity. Notice that this electron curvature drift term is always stabilizing since $\omega_{*e}/\omega_A \ll 1$, where ω_{*e} is the electron diamagnetic drift frequency. The ion contribution can still be neglected, since its thermal velocity is much smaller than the Alfvén phase velocity. Shown in Fig. 5 for CIT parameters is the growth rate of the GAE $(0,-2)$ mode (solid line) with the effect of the electron curvature drift term included; for comparison, the growth rate without the electron drift term (dashed line) is also shown. We observe that for these parameters the electron drift term overcomes the alpha particle term and stabilizes the GAE mode.

To gain a quantitative understanding of the electron drift effect, we again examine the local dispersion relation, including both the alpha particle and electron magnetic drift terms:

$$\gamma/\omega_A = \frac{\beta_\alpha}{2k_\parallel^2 R^2}\left(\frac{\omega_{*\alpha}}{\omega} - \frac{1}{2}\right)\frac{v_A}{v_\alpha}F\left(\frac{2v_A}{v_\alpha}\right)$$

$$-\frac{\beta_e}{2k_\parallel^2 R^2}\frac{v_A}{v_e} - \left(k_r^2 + k_\perp^2\right)\rho_s^2\pi^{1/2}\frac{v_A}{v_e} \tag{20}$$

where we have defined the function $F(u) = (1 + 2u^2 + 4u^4)\exp(-u^2)$. Equation (20) is the same as Eq. (12) except that it includes the electron drift term as well as that of the alpha particles (modeled with a slowing-down distribution). In writing Eq. (20), we have approximated the velocity integral term for the GAE $(0, -2)$ mode as $R_{m+1} + R_{m-1} \approx 2(v_A/v_s)F(2v_A/v_s)$ and also neglected the ω_{*e} term since $\omega_{*e}/\omega_A \ll 1$. Notice that the second term on the right-hand side of Eq. (20) arises from the electron curvature drift, whereas the third term is the usual electron Landau damping due to parallel electron motion, which is smaller by a factor of $\omega_{CA}^2/\omega_{ci}^2 \ll 1$ compared to the second term, where ω_{CA} is the compressional Alfvén frequency. Thus we can estimate the overall electron damping rate as

$$\gamma_e/\omega_A \approx -\frac{\beta_e}{2k_\parallel^2 R^2}\frac{v_A}{v_e} = -1.0 \times 10^{-3} \tag{21}$$

for the GAE $(0, -2)$ mode with CIT parameters. Numerically we obtain $\gamma_e/\omega_A = -1.7 \times 10^{-3}$ and a maximum alpha particle-induced growth rate of $\gamma_\alpha/\omega_A = 1.3 \times 10^{-3}$ at $L_\alpha/a = 0.45$. Therefore the GAE $(0, -2)$ mode is stabilized by the electron damping due to their magnetic curvature drift.

3 GAE Stability in Toroidal Geometry

In the preceeding section, we explored the stability of the GAE in the cylindrical approximation. Here we investigate the effects of toroidicity on the stability of the GAE modes. We will show that in addition to the stabilizing effect of electron curvature drift discussed in Sec. 2.3, toroidicity will enhance the parallel electron Landau damping from sideband Alfvén resonance to the point where the alpha particle-excited GAE modes can be completely stabilized. In order to have a clear physical understanding, here we concentrate on the effects of toroidicity and temporarily drop the stabilizing effects of electron curvature drift.

3.1 Eigenmode Formulation

We start with Ampére's law, Eq. (1). It is convenient to separate the susceptibility tensor $\boldsymbol{\chi}$ into three distinctive parts:

$$\boldsymbol{\chi} = \boldsymbol{\chi}_f + \boldsymbol{\chi}_k + \boldsymbol{\chi}_\alpha \ . \tag{22}$$

Here $\boldsymbol{\chi}_f$ is the bulk plasma fluid response and $\boldsymbol{\chi}_k$ is the bulk plasma kinetic response, which includes finite ion Larmor radius effects and parallel electron dynamics. The following form of $\boldsymbol{\chi}_f$ can be derived from the ideal MHD equations:

$$\boldsymbol{\chi}_f = \frac{c^2}{v_A^2}(\mathbf{I} - \mathbf{bb}) \ , \tag{23}$$

where $\mathbf{I}$ is the unit tensor. To have a clear physical picture, we rewrite Ampére's law in the following form:

$$\left(\nabla \times \nabla \times -\frac{\omega^2}{c^2}\boldsymbol{\chi}_f\right)\mathbf{E} = (\boldsymbol{\chi}_k + \boldsymbol{\chi}_\alpha)\,\mathbf{E} \tag{24}$$

where the terms on the left-hand side correspond to the ideal MHD dynamics, and the terms on the right-hand side represent the kinetic effects of both the bulk component and the alpha particles, respectively. In toroidal geometry, all the terms in Eq. (24) contain some mode coupling. Here we keep only the coupling from the left-hand side of Eq. (24) and neglect the toroidicity effects contained in the kinetic response from the cold component and alpha particles. This approximation may be justified for the following reasons. The mode coupling from the alpha particles is small because of the ordering $\beta_\alpha \ll 1$. Also, the kinetic term $\boldsymbol{\chi}_k$ is small except near the shear-Alfvén resonance, so we can neglect the toroidicity contribution from $\boldsymbol{\chi}_k$, at least away from the Alfvén resonance. Furthermore, we find that near the resonance the kinetic mode coupling can also be neglected, since the $\mathcal{O}(\varepsilon)$ mode coupling contributions due to the $\frac{\omega^2}{v_A^2}$ and $k_\parallel^2$ terms combine and therefore are larger than the corresponding kinetic mode coupling contribution. Hence, we may use the cylindrical form of $\boldsymbol{\chi}_k$ in Eq. (24).

To simplify the mode coupling due to the operator term $\nabla \times \nabla \times$ and the $\boldsymbol{\chi}_f$ term, we assume concentric circular flux surfaces and use the following toroidal coordinates:

$$\begin{cases} x = R\cos(-\varphi) \\ y = R\sin(-\varphi) \\ z = r\sin\theta \\ R = R_0 + r\cos\theta \end{cases}$$

In terms of this toroidal coordinate system and with the representation $\mathbf{E} = (E_r, E_\perp, E_\parallel)$ for the electric field, we find the components of $\nabla \times \nabla \times \mathbf{E}$ to be

$$(\nabla \times \nabla \times \mathbf{E})_r = \left(\frac{1}{R^2}\frac{\partial^2}{\partial\varphi^2} + \frac{1}{r^2 R}\frac{\partial}{\partial\theta}R\frac{\partial}{\partial\theta}\right)E_r +$$

$$\left(-\frac{1}{r^2 R}\frac{\partial}{\partial\theta}R\frac{\partial}{\partial r}\frac{r}{\sqrt{1+\delta^2}} + \frac{1}{R^2}\frac{\partial}{\partial\varphi}\frac{\partial}{\partial r}\frac{R\delta}{\sqrt{1+\delta^2}}\right)E_\perp -$$

$$\left(\frac{1}{rR}\frac{\partial}{\partial\theta}R\frac{\partial}{\partial r}\frac{r\delta}{\sqrt{1+\delta^2}} + \frac{1}{R^2}\frac{\partial}{\partial\varphi}\frac{\partial}{\partial r}\frac{R}{\sqrt{1+\delta^2}}\right)E_\parallel \tag{25}$$

$$(\nabla \times \nabla \times \mathbf{E})_\perp = \left(-\frac{1}{R\sqrt{1+\delta^2}}\frac{\partial}{\partial r}\frac{R}{r}\frac{\partial}{\partial\theta} + \frac{\delta}{r\sqrt{1+\delta^2}}\frac{\partial}{\partial r}\frac{r}{R}\frac{\partial}{\partial\varphi}\right)E_r +$$

$$\left[\frac{1}{R\sqrt{1+\delta^2}}\left(\frac{\partial}{\partial\varphi}+\frac{1}{q}\frac{\partial}{\partial\theta}\right)\frac{1}{R}\left(\frac{\partial}{\partial\varphi}+\frac{1}{q}\frac{\partial}{\partial\theta}\right)\frac{1}{\sqrt{1+\delta^2}} + \right.$$

$$\left.\frac{1}{R\sqrt{1+\delta^2}}\frac{\partial}{\partial r}\frac{R}{r}\frac{\partial}{\partial r}\frac{r}{\sqrt{1+\delta^2}} + \frac{\delta}{r\sqrt{1+\delta^2}}\frac{\partial}{\partial r}\frac{r}{R}\frac{\partial}{\partial r}\frac{R\delta}{\sqrt{1+\delta^2}}\right]E_\perp +$$

$$\left[\frac{1}{R\sqrt{1+\delta^2}}\left(\frac{\partial}{\partial\varphi}+\frac{1}{q}\frac{\partial}{\partial\theta}\right)\frac{1}{rR}\left(\delta^2 q\frac{\partial}{\partial\varphi}-\frac{\partial}{\partial\theta}\right)\frac{R}{\sqrt{1+\delta^2}} + \right.$$

$$\left.\frac{1}{R\sqrt{1+\delta^2}}\frac{\partial}{\partial r}\frac{R}{r}\frac{\partial}{\partial r}\frac{r\delta}{\sqrt{1+\delta^2}} - \frac{\delta}{r\sqrt{1+\delta^2}}\frac{\partial}{\partial r}\frac{r}{R}\frac{\partial}{\partial r}\frac{R}{\sqrt{1+\delta^2}}\right]E_\parallel \tag{26}$$

with $\delta = r/qR$. It is straightforward to show that the infinite aspect ratio limit of Eqs. (25) and (26) — i.e., with R replaced by R_0 — reduces to exactly the same equations as were

derived by Ross *et al.* for cyindrical geometry [cf. Eq. (1) of Ref. 13]. Following Ref. 13, we shall not make use of the parallel component of Ampere's law; instead, as before, $E_{||}$ can be eliminated in terms of E_r and $E_\perp$ by means of $\nabla \cdot \mathbf{J} = 0$:

$$E_{||} = -\frac{B}{\chi_{||,||}} \left(R^2 \mathbf{B} \cdot \nabla \right)^{-1} \left(R^2 \nabla \cdot (\boldsymbol{\chi} \cdot \mathbf{E})_\perp \right) \ . \tag{27}$$

Notice that the operator $R^2\mathbf{B} \cdot \nabla = R_0 B_0 (\partial/\partial\varphi + \partial/q\partial\varphi)$ contains no toroidicity, and hence we can invert it algebraically. In any case, we will neglect the toroidicity due to $E_{||}$ terms since these are kinetic terms.

In this way, we eventually find that Eq. (24) can be rewritten in the same form as that of Eq. (2), but now the operator $\tilde{L}$ contains toroidal coupling. It can be expanded straightforwardly, with the inverse aspect ratio $\varepsilon = a/R$ as a small parameter:

$$\tilde{L} = \tilde{L}_0 + \varepsilon \frac{r}{a} (2 \cos\theta \tilde{L}_S + 2i \sin\theta \tilde{L}_A) \tag{28}$$

Here $\tilde{L}_0$ is the cylindrical operator and is the same as that given in Eqs. (2)–(6). The toroidal terms $\tilde{L}_S$ and $\tilde{L}_A$ are given by

$$(\tilde{L}_S)_{rr} = -\frac{1}{R_0^2} \frac{\partial^2}{\partial\varphi^2}$$

$$(\tilde{L}_S)_{r\perp} = -\frac{1}{2r^3} \frac{\partial}{\partial\theta} \frac{\partial}{\partial r} r^2 \delta_0^2 - \frac{1}{R_0} \frac{\partial}{\partial\varphi} \frac{\partial}{\partial r} \frac{\delta_0}{\sqrt{1+\delta_0^2}}$$

$$(\tilde{L}_S)_{\perp r} = -\frac{1}{2} \left(\frac{1}{\sqrt{1+\delta_0^2}} - \delta_0^2 + \frac{\delta_0^2}{r} \frac{\partial}{\partial r} \right) \frac{\partial}{\partial\theta} - \frac{\delta_0}{r R_0 \sqrt{1+\delta_0^2}} \left(\frac{3}{2} + r \frac{\partial}{\partial r} \right) \frac{\partial}{\partial\varphi}$$

$$(\tilde{L}_S)_{\perp\perp} = \frac{1}{2} \left[\delta_0^2 \frac{\partial}{\partial r} \frac{1}{r} \frac{\partial}{\partial r} \frac{r}{\sqrt{1+\delta_0^2}} + \frac{1}{r\sqrt{1+\delta_0^2}} \frac{\partial}{\partial r} \frac{1}{r} \frac{\partial}{\partial r} r^2 \delta_0^2 \right.$$

$$\left. + \frac{1}{r^2\sqrt{1+\delta_0^2}} \frac{\partial}{\partial r} \frac{r}{\sqrt{1+\delta_0^2}} - \frac{\delta_0}{r\sqrt{1+\delta_0^2}} \frac{\partial}{\partial r} \frac{\delta_0}{\sqrt{1+\delta_0^2}} \right.$$

$$- \frac{2\delta_0}{r\sqrt{1+\delta_0^2}} \frac{\partial}{\partial r} r \frac{\partial}{\partial r} \frac{\delta_0}{\sqrt{1+\delta_0^2}}\Bigg] - \frac{1}{R_0^2}\left(\frac{\partial}{\partial\varphi} + \frac{1}{q}\frac{\partial}{\partial\theta}\right)^2$$

$$(\tilde{L}_A)_{rr} = \frac{i}{2r^2}\frac{\partial}{\partial\theta}$$

$$(\tilde{L}_A)_{r\perp} = -i2\left(\frac{1}{r^2}\frac{\partial}{\partial r}\frac{r}{\sqrt{1+\delta_0^2}} + \frac{1}{r^3}\frac{\partial}{\partial r} r^2\delta_0^2\right)$$

$$(\tilde{L}_A)_{\perp r} = 0$$

$$(\tilde{L}_A)_{\perp\perp} = -\frac{i\delta_0}{4rR_0\sqrt{1+\delta^2}}\left(\frac{\partial}{\partial\varphi} + \frac{1}{q}\frac{\partial}{\partial\theta}\right) .$$

Under Fourier transformation and keeping only nearest-neighbor sideband coupling, we find that Eq. (24) then becomes an infinite set of coupled equations:

$$\hat{\varepsilon}(\tilde{L}_S + \tilde{L}_A)_{m-1}\tilde{E}_{m-1} + (\tilde{L}_0)_m\tilde{E}_m + \hat{\varepsilon}(\tilde{L}_S - \tilde{L}_A)_{m+1}\tilde{E}_{m+1} = 0 \tag{29}$$

where $\hat{\varepsilon} = \varepsilon r/a$. In the limit of $\varepsilon \to 0$, Eq. (29) reduces to the cylindrical form, i.e., $\tilde{L}_{0m}\tilde{E}_m = 0$. For nonzero ε, we have an infinite series of coupled equations. To truncate this infinite series, we consider only three poloidal modes. This is consistent with expanding only to first order in ε. Thus, we finally obtain the following six-by-six matrix of coupled second-order differential equations to be solved numerically:

$$\begin{pmatrix} (\tilde{L}_0)_{m-1} & \hat{\varepsilon}(\tilde{L}_S - \tilde{L}_A)_m & 0 \\ \hat{\varepsilon}(\tilde{L}_S + \tilde{L}_A)_{m-1} & (\tilde{L}_0)_m & \hat{\varepsilon}(\tilde{L}_S - \tilde{L}_A)_{m+1} \\ 0 & \hat{\varepsilon}(\tilde{L}_S + \tilde{L}_A)_m & (\tilde{L}_0)_{m+1} \end{pmatrix} \begin{pmatrix} \tilde{E}_{m-1} \\ \tilde{E}_m \\ \tilde{E}_{m+1} \end{pmatrix} = 0 . \tag{30}$$

3.2 Numerical Results and Discussion

Here we consider the $(1, -2)$ mode as a typical GAE mode with $n \neq 0$, for CIT parameters. The cylindrical results of this mode have already been described in Sec. 2. Notice that

the value of the edge density is not zero, in order to have the Alfvén frequency be finite at the edge. Also we choose the edge density value to be small enough for a sideband resonance to exist. For the sake of comparison and of numerical calculation, we use ε as an independent variable in Eq. (30). Thus, for $\varepsilon = 0$, our calculation will recover the cylindrical eigenvalues. The known cylindrical eigenvalues will then provide us with very good guesses for the corresponding toroidal eigenvalues, which can be traced as the value of ε is increased.

Shown in Fig. 6 is the radial electric field for the main poloidal mode $(1, -2)$ and its two sidebands $(1, -1)$ and $(1, -3)$, for $\varepsilon = 0.1$. Figure 7 shows the sideband $(1, -1)$ for various values of the toroidicity parameter ε. Figure 8 shows both the Landau damping rate obtained without alpha particles, as well as the growth rate induced by alpha particles, with $L_\alpha/a = 0.25$. Note that this value for the alpha particle density scale length L_α corresponds to the maximum growth rate in the cylindrical limit, as shown in Fig. 3(a).

The following observations emerge after examining these results:

(1) The structure of the sideband $(1, -1)$ near its Alfvén resonance has two distinctive types of behavior depending on the value of ε. For small values, (viz., $\varepsilon < 0.3$), the sideband $(1, -1)$ is like an Airy function and the mode propagates toward the center of the plasma. In fact, Stix[22] has shown that for $\beta_e/(m_e/m_i) > 1$ at the resonance, the essential evanescent compressional wave at the edge of the plasma will convert to a kinetic Alfvén wave, which propagates toward the high density region. Our results confirm this physical process. Furthermore, as ε increases, we observe that the sideband resonance shifts toward the edge of the plasma. As a result, the value of $\beta_e/(m_e/m_i)$ at the resonance decreases and eventually becomes less than unity, at which point the KAW becomes the so-called cold surface Alfvén wave.[13,22] Notice that the toroidal coupling will lower the $(1, -1)$ Alfvén continuum, and therefore its resonance moves toward the outside as ε increases. Finally, for $\varepsilon = 0.48$, which corresponds to the CIT value, the $(1, -1)$ singularity simply disappears.

(2) More or less related to the above observations, we note that there are three distinct

stages for the Landau damping rate γ_L and the total growth rate γ including the alpha particles. For small values of $\varepsilon < 0.1$, we find the scalings $\gamma_L \propto \varepsilon^2$ and $\gamma \propto \varepsilon^2$; for intermediate values of ε, $0.1 < \varepsilon < 0.2$, we find that both scale linearly, $\gamma_L \propto \varepsilon$ and $\gamma \propto \varepsilon$; for still larger values, $\varepsilon > 0.25$, γ_L eventually saturates and begins to decrease, while the trend for γ is exactly the opposite.

Recall that the electron Landau damping rate for the localized KAW mode is much higher than that for the GAE modes. Thus the toroidal GAE mode, which is a mixture of the cylindrical GAE mode and a sideband KAW mode, has a greater damping rate. On the other hand, the KAW sideband should contribute little to the alpha particle destabilization since it is localized near the edge of the plasma where few alpha particles reside. Therefore, as ε increases, the electron Landau damping is enhanced and the total growth rate decreases. For $\varepsilon = 0.1$, the mode is stabilized. However, as the value of ε is raised further, the Landau damping begins to saturate and, eventually, to decrease; consequently, the stabilization through toroidal coupling is weakened. The reason for the reduction in the Landau damping is the shifting of the $(1, -1)$ resonance toward the edge of the plasma as ε increases; correspondingly, the coupling between the GAE mode and the KAW sideband is reduced. For the CIT value of $\varepsilon = 0.48$, the GAE mode is still stabilized. Moreover, the inclusion of the additional sideband $(1, 0)$ is expected to shift the $(1, -1)$ resonance toward the center of the plasma, as opposed to the $(1, -2)$ mode. Thus we expect the stabilizing effect to be further enhanced.

At this point, it is instructive to apply quantum mechanical perturbation theory to our mode coupling problem. In previous work[23] the toroidal Alfvén modes had been analytically constructed by means of a superposition of cylindrical eigenmodes in the ideal MHD limit. In the present theory, however, kinetic effects are included in our eigen-equation. Our problem is similar to a quantum mechanical system in the following sense. Equation (30) can be viewed as an eigenvalue equation, with the diagonal elements as the unperturbed operators and the

off-diagonal elements as the perturbation. In the limit of $\varepsilon \to 0$ or zero perturbation, the eigenvalue of our system reduces to the unperturbed spectrum or the cylindrical spectrum. Making the analogy with quantum mechanical perturbation theory, we can now reproduce the scaling of the frequency shift and the sideband amplitude due to toroidicity. For small ε, the unperturbed spectrum is non-degenerate; consequently the amplitude of the perturbed sideband is proportional to ε and the frequency shift $\delta\omega$ has the scaling $\delta\omega \propto \varepsilon^2$. As ε is increased, the spectrum becomes degenerate and we must invoke the method of degenerate perturbation theory. In this case, we have the linear scaling $\delta\omega \propto \varepsilon$. These analytical scalings agree well with our numerical results for $\varepsilon < 0.2$.

We also considered GAE modes with $n = 0$. In particular, we found that the $(0, -2)$ mode can also stabilized by toroidicity. However, for $n = 0$ modes, two sidebands are no longer adequate to describe the toroidal coupling. The reason[25,26] is that in the MHD limit, the $(0, -m)$ mode and the $(0, m)$ mode have equal amplitude, and hence the destabilizing alpha particle source is eliminated due to cancellation between the $\omega_{*\alpha,m}$ and $\omega_{*\alpha,-m}$ terms. Therefore, complete toroidal coupling for the $(0, -m_c)$ cylindrical GAE mode must include at least the harmonics with poloidal mode number from $m = -(m_c + 1)$ to $m = m_c + 1$. harmonics. This has been done in the work reported in Refs. 25 and 26, where all necessary poloidal harmonics were included for the $n = 0$ GAE modes, but in the MHD limit.

4 Conclusion

In this work, we have studied the stability of the Global Alfvén Eigenmodes in the presence of fusion alpha particles in an ignited tokamak plasma. In the cylindrical approximation, we found that alpha particle destabilization of GAE modes is significantly enhanced when the alpha particles are modeled with a slowing-down distribution function rather than with a Maxwellian. On the other hand, we found that the electron damping due to the magnetic curvature drift contribution is stabilizing and can, in fact, be comparable to the magnitude

of the destabilizing alpha particle term. In particular, for CIT parameters, the GAE modes is stabilized by this electron damping. In toroidal geometry, the intrinsic toroidicity induces poloidal mode couping, which enhances the parallel electron damping from the sideband shear-Alfvén Landau resonance. As a result, we found that toroidicity can stabilize the GAE modes for CIT parameters. We conclude that the GAE modes will be stable in a typical ignited tokamak plasma.

The results of this work have several important implications. With regard to Alfvén wave heating, the sideband resonance may lead to substantial edge heating, which is very unfavorable. In the case of tokamak divertor operation, the toroidal mode coupling is expected to be even stronger and more complex since the magnetic surfaces are now elongated and a magnetic flux separatrix exists at the edge of the plasma. Much work is needed in this area. Another important aspect of toroidal coupling is the so-called discrete Toroidicity-Induced Shear Alfvén Eigenmode (TAE),[27,28] whose frequency lies within toroidicity-induced gaps in the Alfvén continuum. This new toroidal global mode has a parallel wave length that is typically longer than that of the cylindrical GAE mode and therefore is more easily destabilized by alpha particles. We have shown that TAE modes can in fact be strongly destabilized by alpha particles for a typical ignited tokamak.[24–26] The complete results will be reported elsewhere.[29] Thus, even though the present work indicates that the GAE modes are likely not to be a threat in ignited tokamak plasmas, these toroidicity-induced TAE modes could be quite problematic.

Acknowledgments

The authors gratefully acknowledge helpful discussions with Drs. M.N. Rosenbluth, D.W. Ross, H.L. Berk, C.Z. Cheng, and K. Appert. One of the authors (G.Y.F.) especially thanks Prof. M.N. Rosenbluth for suggesting this work, Dr. D.W. Ross for the loan of the Alfvén wave kinetic code, and Prof. H.L. Berk for pointing out the importance of the electron damp-

ing due to the magnetic curvature drift. This work was supported by the U.S. Department of Energy under contract DE-FG-05-80ET-53088 and also by the Texas Advanced Technology Program and the Texas Atomic Energy Research Foundation.

1. K. McGuire, R. Goldston, M. Bell, M. Bitter, K. Bol, K. Brau, D. Buchenauer, T. Crowley, S. Davis, F. Dylla, H. Eubank, H. Fishman, R. Fonck, B. Grek, R. Grimm, R. Hawryluk, H. Hsuan, R. Hulse, R. Izzo, R. Kaita, S. Kaye, H. Kugel, D. Johnson, J. Manickam, D. Manos, D. Mansfield, E. Mazzucato, R. McCann, D. McCune, D. Monticello, R. Motley, D. Mueller, K. Oasa, M. Okabayashi, K. Owens, W. Park, M. Reusch, N. Sauthoff, G. Schmidt, S. Sesnic, J. Strachan, C. Surko, R. Slusher, H. Takahashi, F. Tenney, P. Thomas, H. Towner, J. Valley, and R. White, Phys. Rev. Lett. **50**, 891 (1983).

2. L. Chen, R.B. White, and M.N. Rosenbluth, Phys. Rev. Lett. **52**, 1122 (1984).

3. J. Weiland and L. Chen, Phys. Fluids **28**, 1359 (1985).

4. J.W. Van Dam, M.N.Rosenbluth, H.L. Berk, N. Dominguez, G.Y. Fu, X. Llobet, D.W. Ross, D.P. Stotler, D.A. Spong, W.A. Cooper, D.J. Sigmar, D.E. Hastings, J.J. Ramos, H. Naito, T. Todoroki, S.T. Tsai, S.G. Guo, and J.W. Shen, in *Plasma Physics and Controlled Nuclear Fusion Research 1986* (IAEA, Vienna, 1987), vol. 2, p. 135.

5. M.N. Rosenbluth, S.T. Tsai, J.W. Van Dam, and M. G. Engquist, Phys. Rev. Lett. **51**, 1967 (1983).

6. R.B. White, M.N. Bussac, and F. Romanelli, Princeton Plasma Physics Laboratory Report PPPL-2540 (1988).

7. F. Pegoraro, F. Porcelli, and J. Hastie, Sherwood Theory Conference, Gatlinburg, TN, 1988, paper 2B1.

8. Y.Z. Zhang, H.L. Berk, and S.M. Mahajan, Institute for Fusion Studies Report IFSR-326 (1988), accepted for publication in Nucl. Fusion.

9. E.M. Barston, Ann. Phys. (N.Y.), **29**, 282 (1964).

10. Z. Sedlacek, J. Plasma Phys. **5**, 239 (1971).

11. L. Chen and A. Hasegawa, Phys. Fluid **17**, 1399 (1974).

12. K. Appert, R. Gruber, F. Troyon, and J. Vaclavik, Plasma Phys. **24**, 1147 (1982).

13. D.W. Ross, G.L. Chen, and S.M. Mahajan, Phys. Fluids **25**, 652 (1982).

14. S.M. Mahajan, D.W. Ross, and G.L. Chen, Phys. Fluids **26**, 2195 (1983)

15. S.M. Mahajan, Phys. Fluids **27**, 2238 (1984).

16. R. Behn, A. de Chambrier, G.A. Collins, P.-A. Duperrex, A. Heym, F. Hofmann, Ch. Hollenstein, B. Joye, R. Keller, A. Lietti, J.B. Lister, J.-M. Moret, S. Nowak, J. O'Rourke, A. Pochelon, and W. Simm, Plasma Phys. Contr. Fusion **26**, 173 (1984).

17. T.E. Evans, P.M. Valanju, J.F. Benesch, R.D. Bengtson, Y.-M. Li, S.M. Mahajan, M.E. Oakes, D.W. Ross, Z.-Z. Wang, and J.G. Watkins, Phys. Rev. Lett. **53**, 1743 (1984); R.D. Bengtson, T.E. Evans, Y.-M. Li, S.M. Mahajan, M.E. Oakes, D.W. Ross, C.M. Surko, P.M. Valanju, X.-Z. Wang, and J.G. Watkins, Proc. Fourth Joint Varenna-Grenoble Int. Symposium on Heating in Toroidal Plasma, Roma (International School of Physics, Varenna, 1984), Vol. **1**, p. 121.

18. A.B. Mikhailovskii, Zh. Eksp. Teor. Fiz. **68**, 1772 [Sov. Phys. - JETP **41**, 890 (1975)].

19. M.N. Rosenbluth and P.H. Rutherford, Phys. Rev. Lett. **34**, 1428 (1975).

20. K.T. Tsang, D.J. Sigmar, and J.C. Whitson, Phys. Fluids **24**, 1508 (1981).

21. Y.M. Li, S.M. Mahajan, and D.W. Ross, Phys. Fluids **30**, 1466 (1987).

22. T. H. Stix, in Heating in Toroidal Plasmas (Proc. 2nd Joint Varenna-Grenoble Symposium), ed. E. Canobbio *et al.* (CEC, Brussels, 1980), vol. 2, p. 631.

23. S. Riyopoulos and S. Mahajan, Phys. Fluids **29**, 731 (1986).

24. G.Y. Fu, Ph.D. Thesis, University of Texas at Austin, Institute for Fusion Studies Report No. 325 (1988)

25. G.Y. Fu, J.W. Van Dam, M.N. Rosenbluth, D.W. Ross, Y.Z. Zhang, H.L. Berk, S.M. Mahajan, C.Z. Cheng, R.L. Miller, X.H. Wang, A. Bhattacharjee, M.E. Mauel, and B. Breizman, in Plasma Physics and Controlled Nuclear Fusion Research 1988, Proceedings of the 12th International Conference (Nice, France, October 12-19, 1988), Paper IAEA-CN-50/D-4-11, to be published.

26. C.Z. Cheng, G.Y. Fu, and J.W. Van Dam, Princeton Plasma Physics Laboratory Report No. 2585 (Jan., 1989), to be published in the Proceedings of the Joint Varenna-Lausanne International Workshop on Theory of Fusion Plasmas (October 3-7, 1988, Chexbres, Switzerland)

27. C.Z. Cheng and M.S. Chance, Phys. Fluids **29**, 3695 (1986).

28. C.Z. Cheng, L. Chen, and M.S. Chance, Ann. Phys. (NY) 161, 21(1984)

29. G.Y. Fu and J.W. Van Dam, Institute for Fusion Studies Report IFSR-368 (1989), submitted to Phys. Fluids B.

Figure Captions

1. Cylindrical shear-Alfvén continua for mode numbers $n = 1$ and $m = -1, -2$, and -3.

2. Numerical eigenfunctions for the cylindrical Global Alfvén Eigenmodes, with CIT parameters: (a) mode $(1, -2)$; (b) mode $(0, -2)$.

3. Growth rate γ for the cylindrical GAE modes as a function of the alpha particle density gradient scale length L_α for a Maxwellian distribution and for a slowing-down distribution, with CIT parameters: (a) mode $(1, -2)$; (b) mode $(0, -2)$.

4. Ratio of $(R_{m\pm1})_{\text{slow}}/(R_{m\pm1})_{\text{Max}}$ and the ratio of $(P_{m\pm1}/R_{m\pm1})_{\text{slow}}$ as functions of the phase $\omega/k_{\|m\pm1}\, v_{\alpha_0}$.

5. Growth rate γ for the cylindrical GAE mode $(0, -2)$, both with the electron curvature drift term (solid curve) and also without this term (dashed curve), as a function of L_α with a slowing-down alpha particle distribution, for CIT parameters.

6. Numerical eigenfunctions for the toroidal GAE mode $(1, -2)$ and the sidebands $(1, -1)$ and $(1, -3)$, with CIT parameters, for the inverse aspect ratio $\varepsilon = 0.1$.

7. Numerical eigenfunctions for the sideband $(1, -1)$ of the toroidal GAE mode $(1, -2)$, with CIT parameters, for the inverse aspect ratio values of $\varepsilon = 0.05, 0.20, 0.30$, and 0.48.

8. Electron Landau damping rate γ_L and the total growth rate γ (with alpha particles), as functions of the inverse aspect ratio ε for the GAE $(1, -2)$ mode coupled to the sidebands $(1, -1)$ and $(1, -3)$.

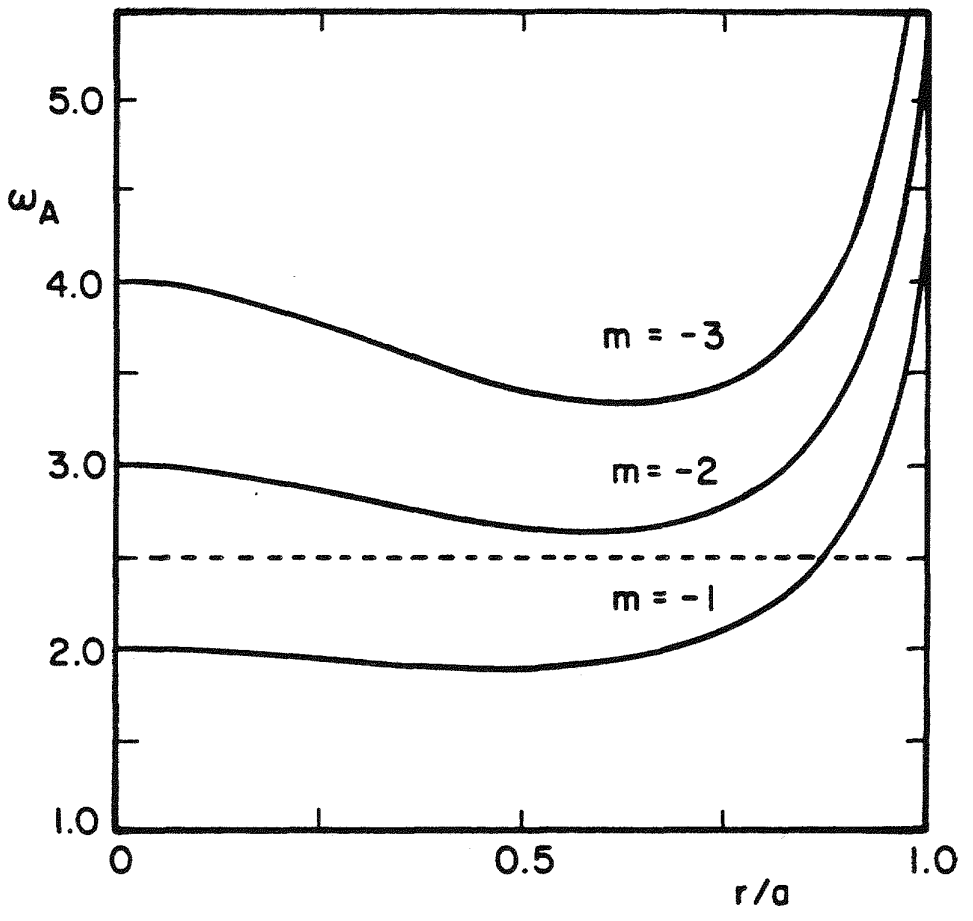

Figure 1

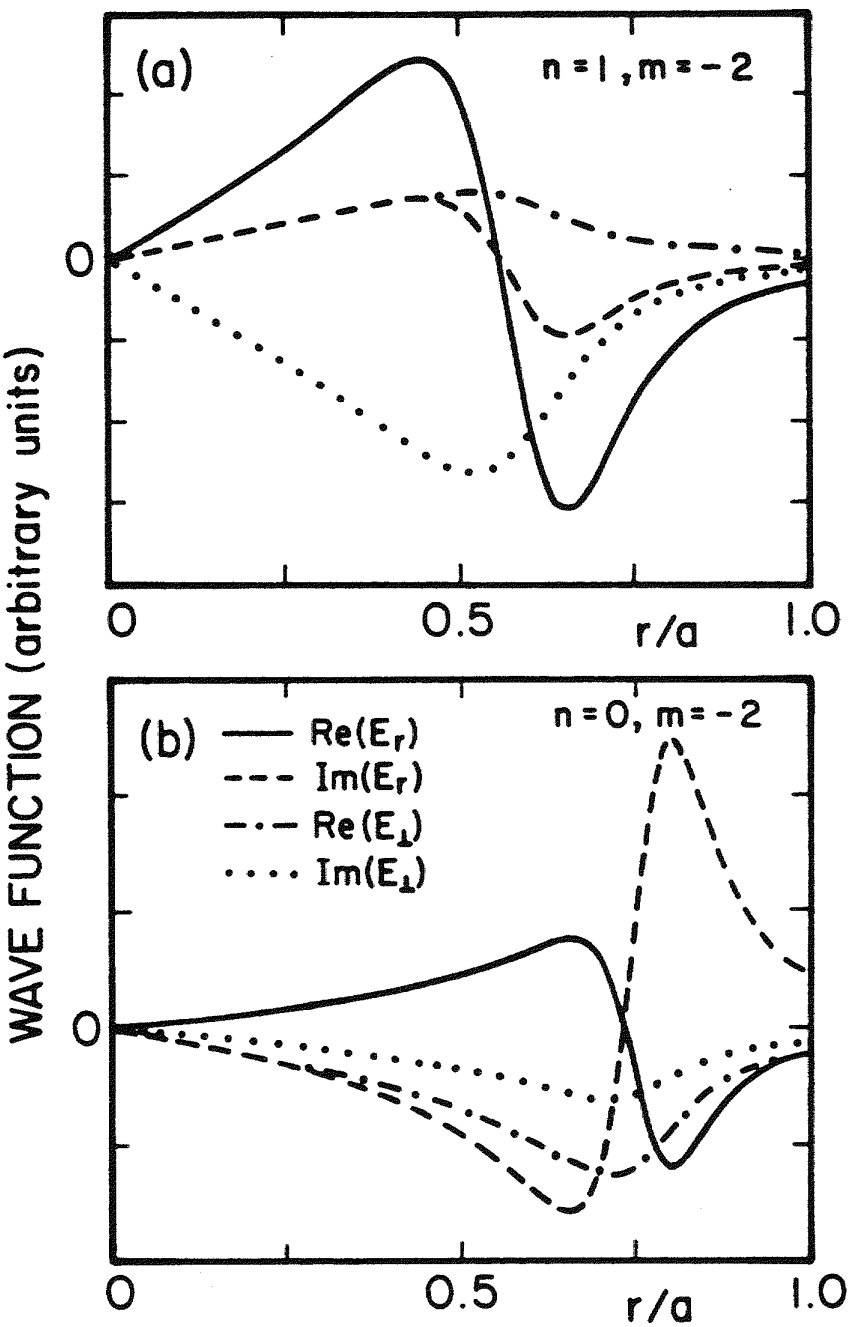
(a)
n = 1, m = -2
0
0
0.5
r/a
1.0
(b)
Re(E_r)
Im(E_r)
Re(E_⊥)
Im(E_⊥)
n = 0, m = -2
WAVE FUNCTION (arbitrary units)
0
0
0.5
r/a
1.0

Figure 2

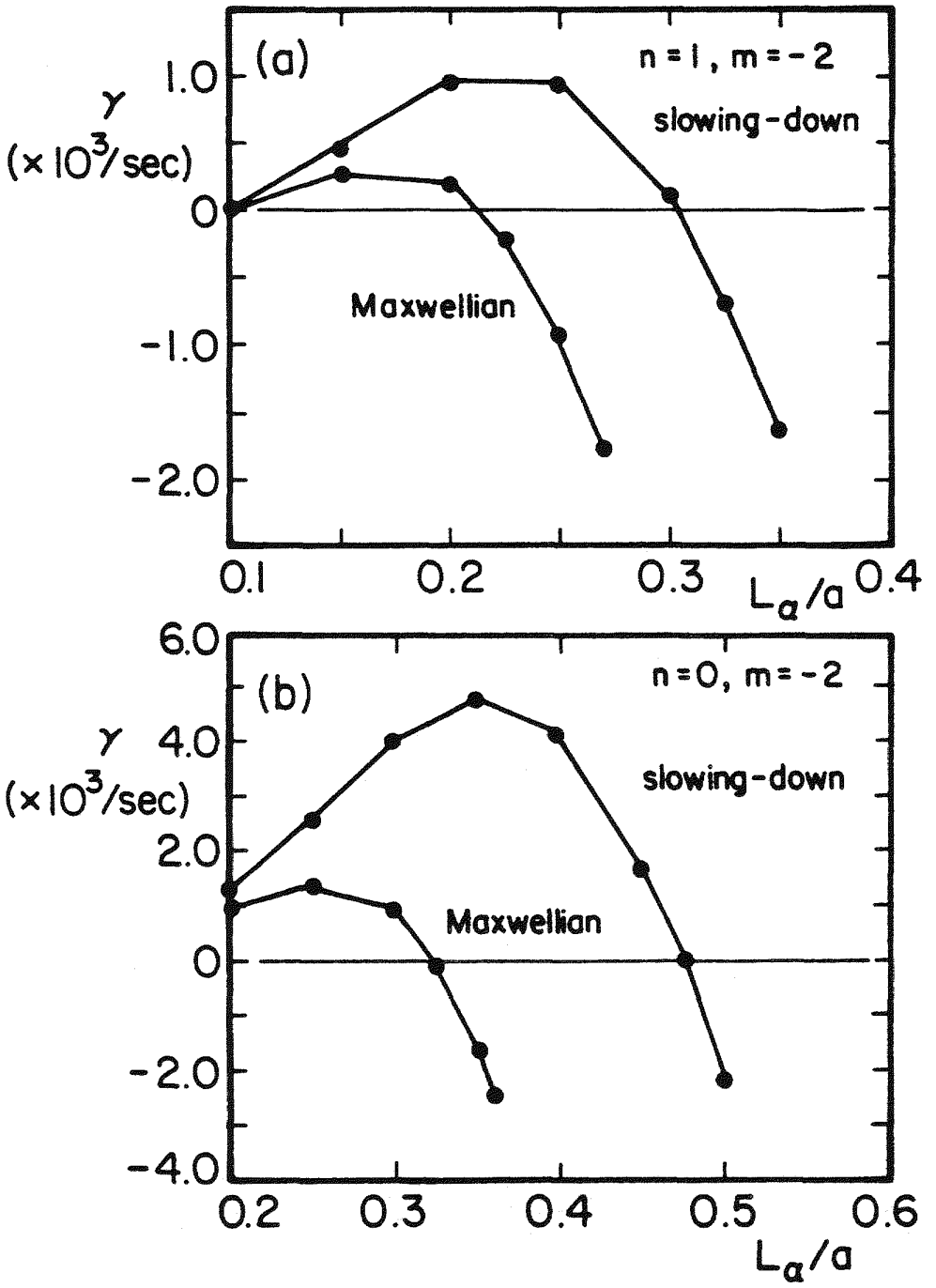
(a)
n = 1, m = -2
slowing-down
Maxwellian
γ
(×10³/sec)
1.0
0
-1.0
-2.0
0.1
0.2
0.3
0.4
L_α/a
(b)
n = 0, m = -2
slowing-down
Maxwellian
γ
(×10³/sec)
6.0
4.0
2.0
0
-2.0
-4.0
0.2
0.3
0.4
0.5
0.6
L_α/a

Figure 3

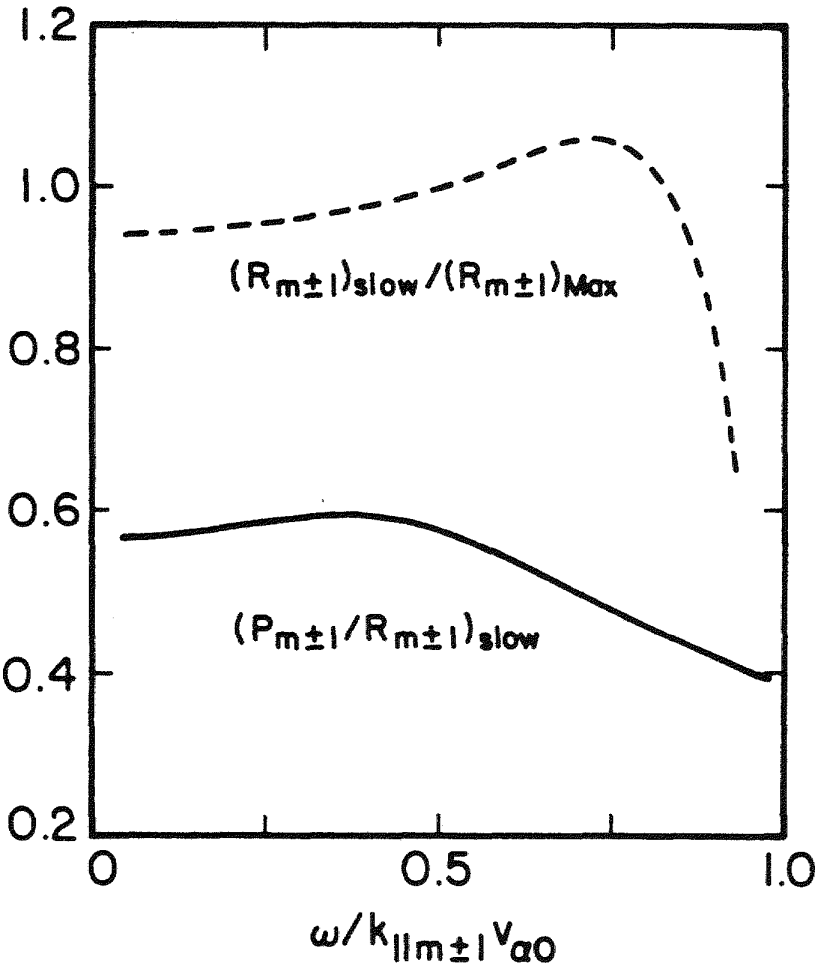
1.2
1.0
0.8
0.6
0.4
0.2
0
0.5
1.0
$(R_{m\pm1})_{slow}/(R_{m\pm1})_{Max}$
$(P_{m\pm1}/R_{m\pm1})_{slow}$
$\omega/k_{\|m\pm1}v_{\alpha0}$

Figure 4

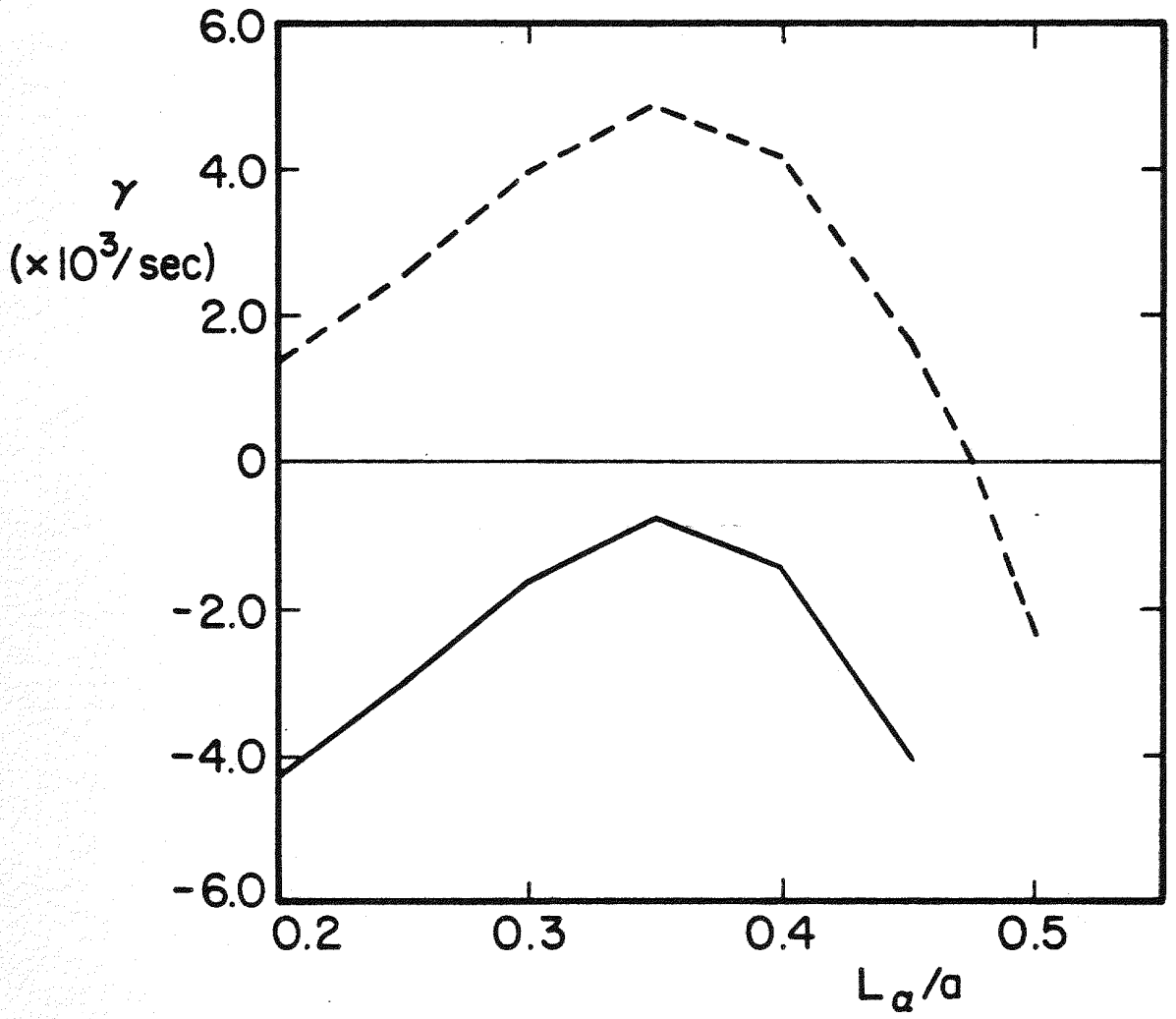

Figure 5

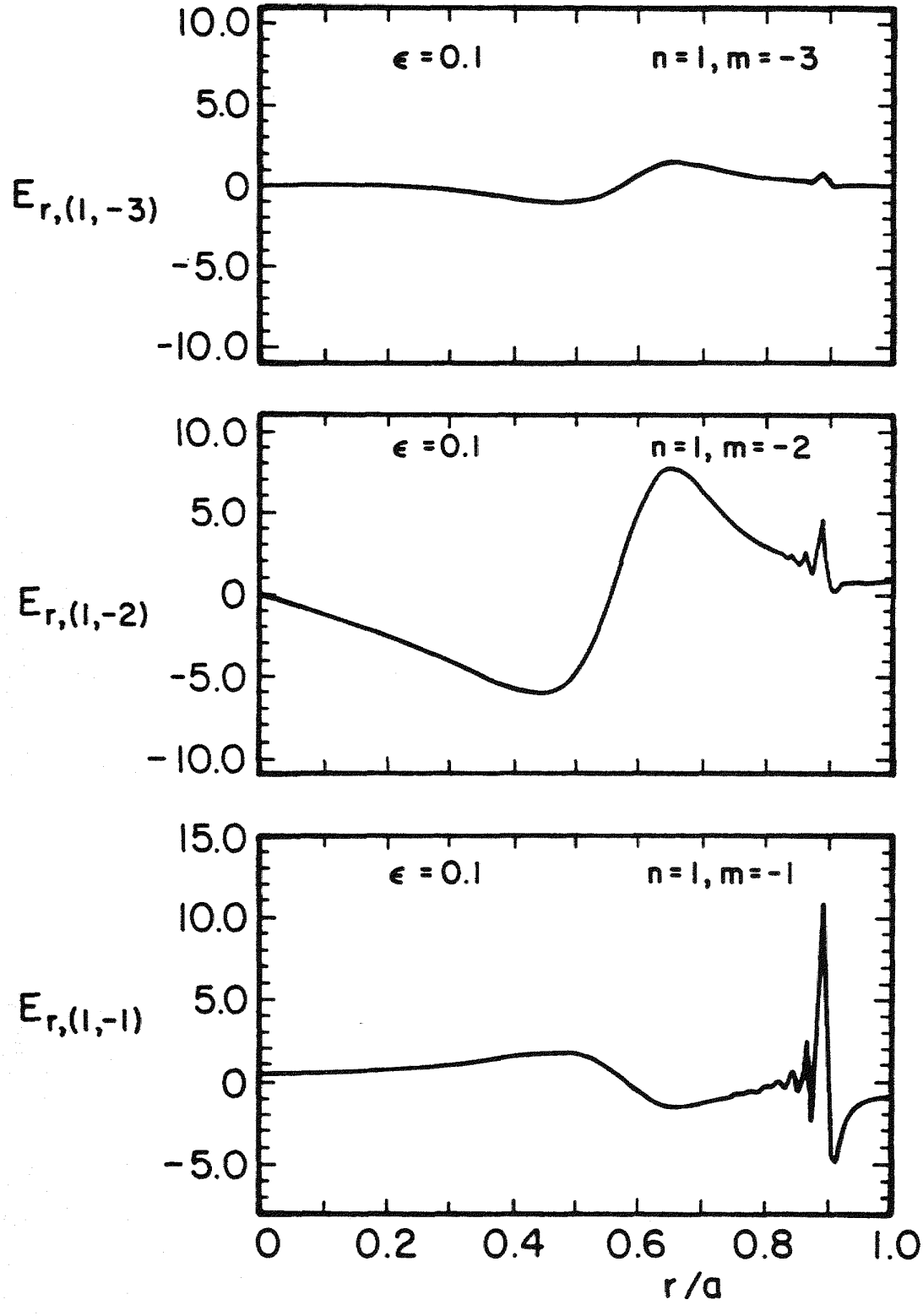
10.0
5.0
0
-5.0
-10.0
ϵ = 0.1
n = 1, m = -3
E r,(1,-3)
10.0
5.0
0
-5.0
-10.0
ϵ = 0.1
n = 1, m = -2
E r,(1,-2)
15.0
10.0
5.0
0
-5.0
ϵ = 0.1
n = 1, m = -1
E r,(1,-1)
0
0.2
0.4
0.6
0.8
1.0
r/a

Figure 6

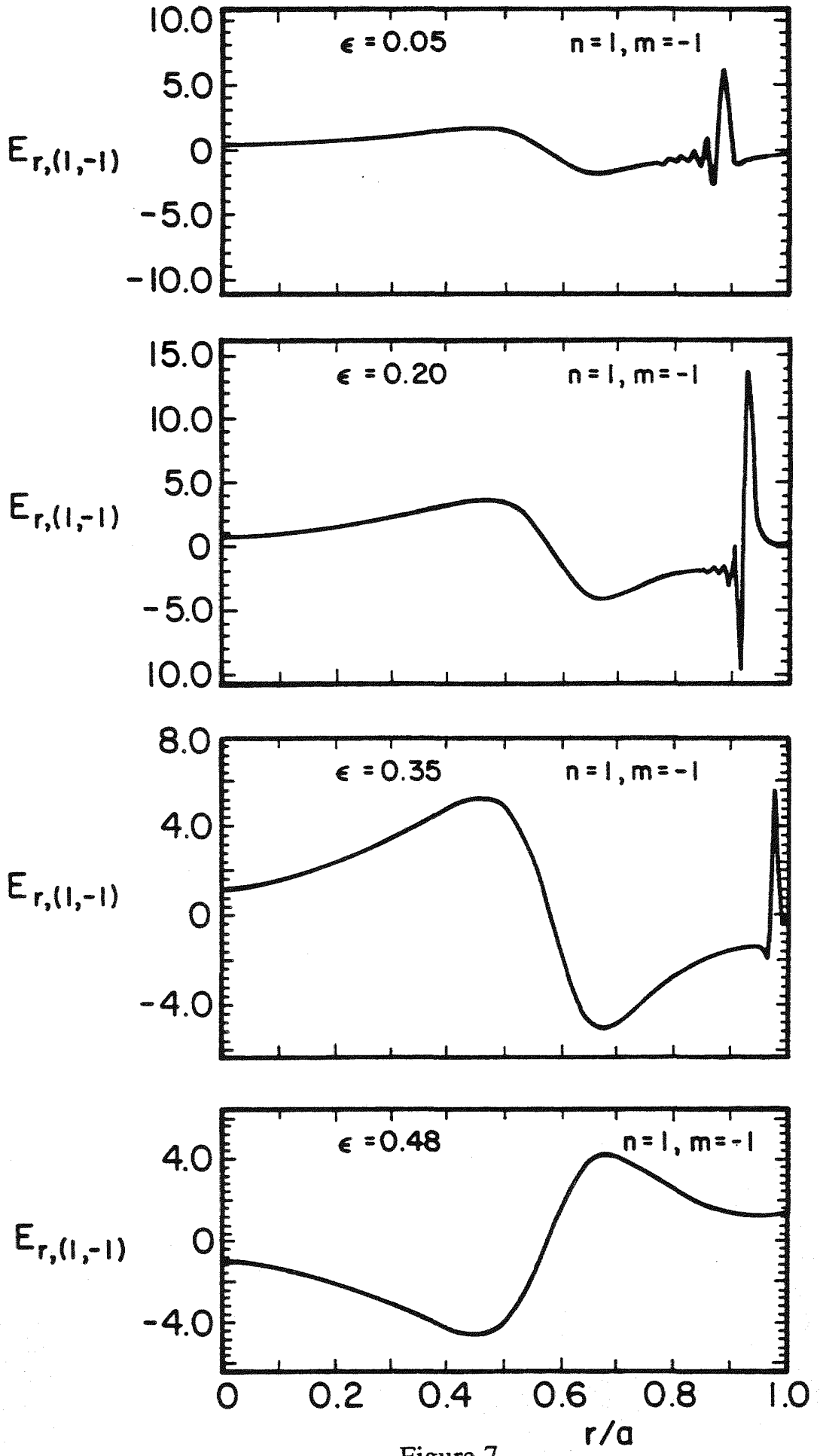
ε = 0.05
n = 1, m = -1
ε = 0.20
n = 1, m = -1
ε = 0.35
n = 1, m = -1
ε = 0.48
n = 1, m = -1
E r,(1,-1)
10.0
5.0
0
-5.0
-10.0
15.0
10.0
5.0
0
-5.0
10.0
8.0
4.0
0
-4.0
4.0
0
-4.0
0
0.2
0.4
0.6
0.8
1.0
r/a

Figure 7

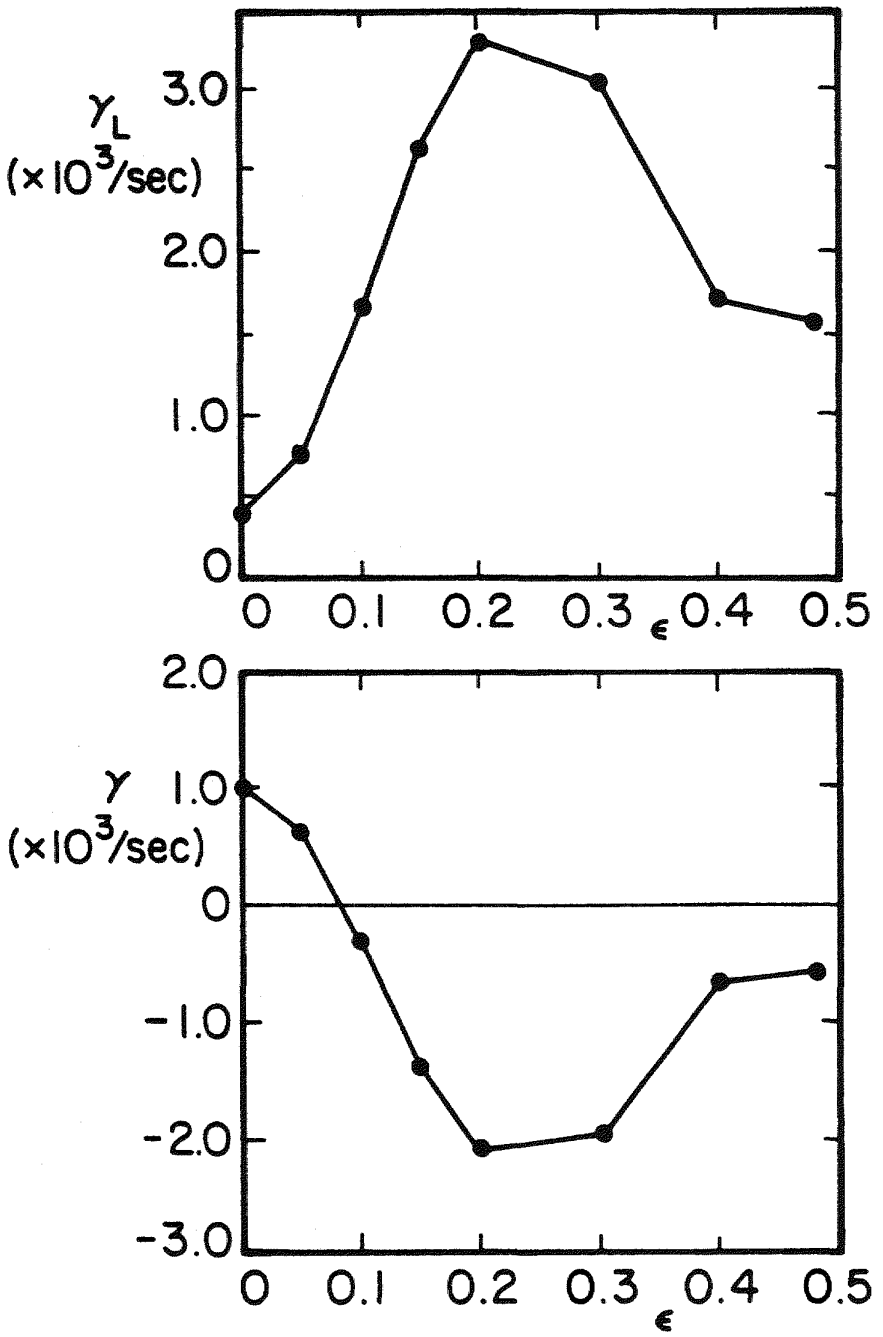
γ_L
(×10³/sec)
3.0
2.0
1.0
0
0
0.1
0.2
0.3
ϵ
0.4
0.5
2.0
γ 1.0
(×10³/sec)
0
-1.0
-2.0
-3.0
0
0.1
0.2
0.3
ϵ
0.4
0.5

Figure 8